Supplement of The Cryosphere, 20, 87–96, 2026
https://doi.org/10.5194/tc-20-87-2026-supplement

The Cryosphere Open Access EGU

Supplement of

Estimating Antarctic surface melt rates using passive microwave data calibrated with weather station observations

Valeria Di Biase et al.

Correspondence to: Valeria Di Biase (vdibiase@edf.org)

SSMIS-based melt indicator	Definition
Pure Brightness Temperature (T_b)	Absolute T_b at each analyzed frequency (19, 37, and 91 GHz), both polarizations, and for both evening and morning overpasses.
Winter Anomaly (A_w)	$$A_w = T_{b,19H}^{(E)} - \mu_{winter}$$ where $T_{b,19H}^{(E)}$ is the 19GHz, H polarization brightness temperature at the evening overpass and μ_{winter} is its mean over winter period. In this work, we defined winter period as 1 June – 31 August.
Diurnal Amplitude (ΔT_d); **Day-to-Day Change** (ΔT_{1d})	$$\Delta T_d = T_{b,19H}^{(E)} - T_{b,19H}^{(M)}$$ Representing the difference between morning (M) and evening (E) overpasses; $$\Delta T_{1d} = T_{b,19H}^{(d)} - T_{b,19H}^{(d-1)}$$ Comparing the same overpass on successive days.
Normalized Polarization Ratio (NPR)	$$NPR_{19} = \frac{T_{b,19V} - T_{b,19H}}{T_{b,19V} + T_{b,19H}}$$ Where $T_{b,19V}$ is the 19 GHz vertical polarization brightness temperature.
Normalized seasonal Anomaly	$$c_w = \frac{T_{b,19H} - A_w}{\sigma_w}$$ $$c_y = \frac{T_{b,19H} - A_w}{\sigma_y}$$ Where σ_w is the standard deviation of 19GHz, H polarization brightness temperatrue during the winter season, and σ_y is the corresponding standard deviation over the entire Antarctic year. c_w and c_y are dimensionless indicators accounting for interannual variability in radiometric response. In literature, once$T_{b,19H}^{(E)}$ is expressed as $A_w + c_w \cdot \sigma_w$, threshold values for c_w typically range from 1.5 to 3. Similarly, an alternative formulation has been tested using c_y in plase of c_w, leveraging the full-year standard deviation to account for broader seasonal fluctuations.

Table S1: Overview of candidate SSMIS-based melt indicators tested in this study. Variables are grouped by physical principle, with corresponding definitions. The equations and descriptions refer primarily to the 19 GHz horizontal polarization case, which yielded the best performance; however, analogous expressions were computed for other frequencies (37 GHz, 91 GHz), overpass times (morning and evening), and polarizations (horizontal and vertical).

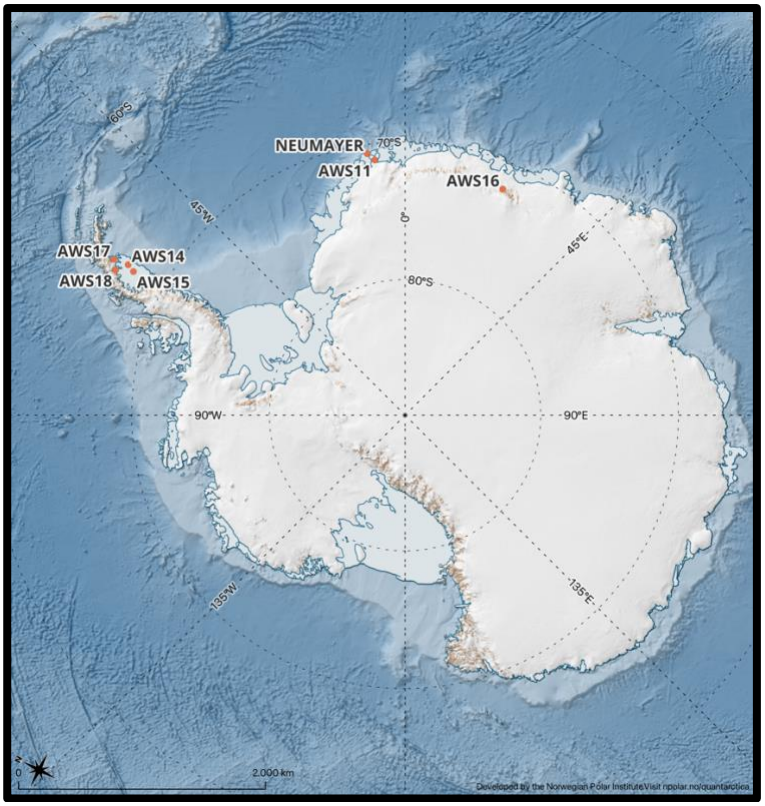

Figure S1. Locations of the automatic weather stations (AWS) used in this study: AWS11 (Halvfarryggen Ice Rise), AWS14 (northern Larsen C Ice Shelf), AWS15 (central Larsen C Ice Shelf), AWS16 (Princess Elisabeth Station), AWS17 (Scar Inlet, remnant of the Larsen B Ice Shelf), and AWS18 (Cabinet Inlet on the western Larsen C Ice Shelf).

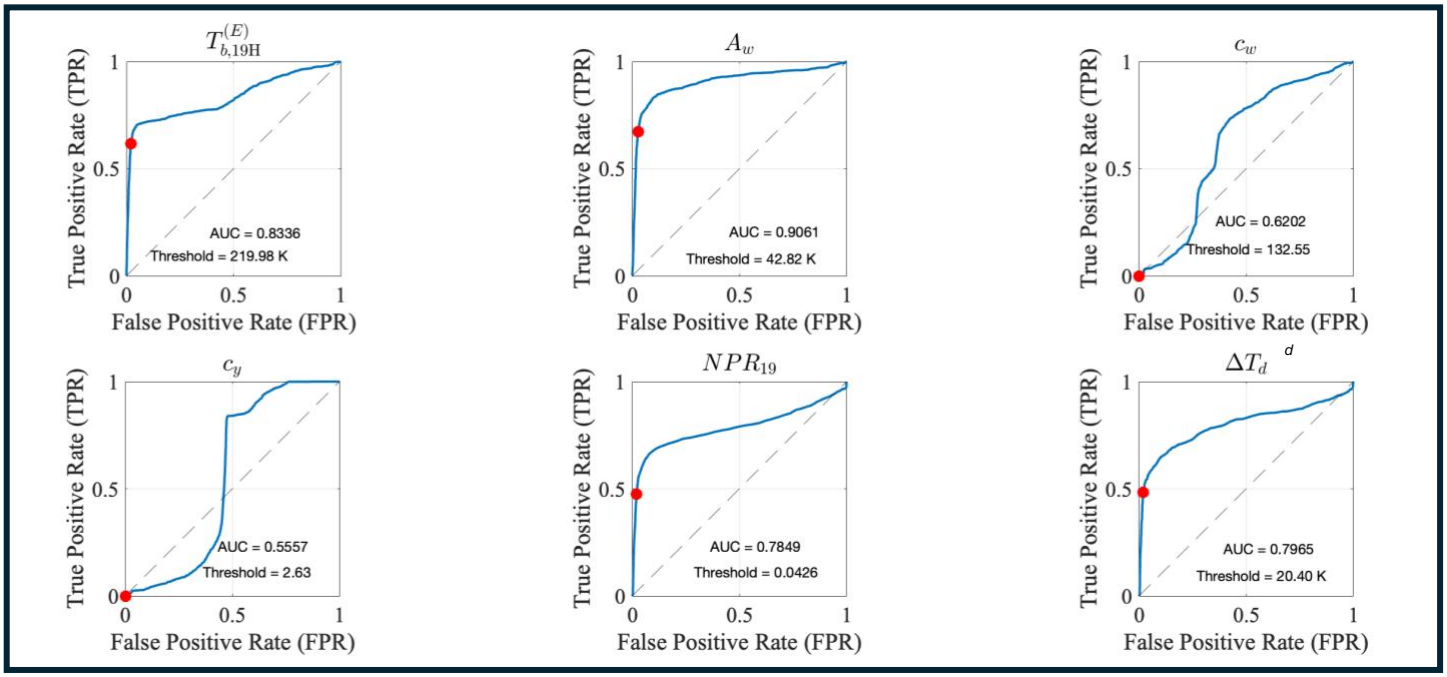

Figure S2. Representative Receiver Operating Characteristic (ROC) curves for the analyzed melt-sensitive indicators (see Tab. S1), each showing the trade-off between true positive rate (TPR) and false positive rate (FPR). Red dots mark the optimal operating point (threshold) for each indicator, and AUC indicates the Area under the Receiver Operating Characteristic Curve.
Indicators shown are:

- **$T^{(E)}_{b,19H}$**: evening overpass brightness temperature at 19 GHz, horizontal polarization
- **A_w**: winter anomaly, defined as $T^{(E)}_{b,19H} - \mu_{winter}$
- **c_w**: winter-season melt index, $(T^{(E)}_{b,19H} - A_w)/\sigma_w$
- **c_y**: annual-scale melt index, $(T^{(E)}_{b,19H} - A_w)/\sigma_y$
- **NPR_{19}**: normalized polarization ratio, $(T_{b,19V} - T_{b,19H})/(T_{b,19V} + T_{b,19H})$
- **ΔT_d**: diurnal amplitude at 19 GHz, $T^{(E)}_{b,19H} - T^{(M)}_{b,19H}$

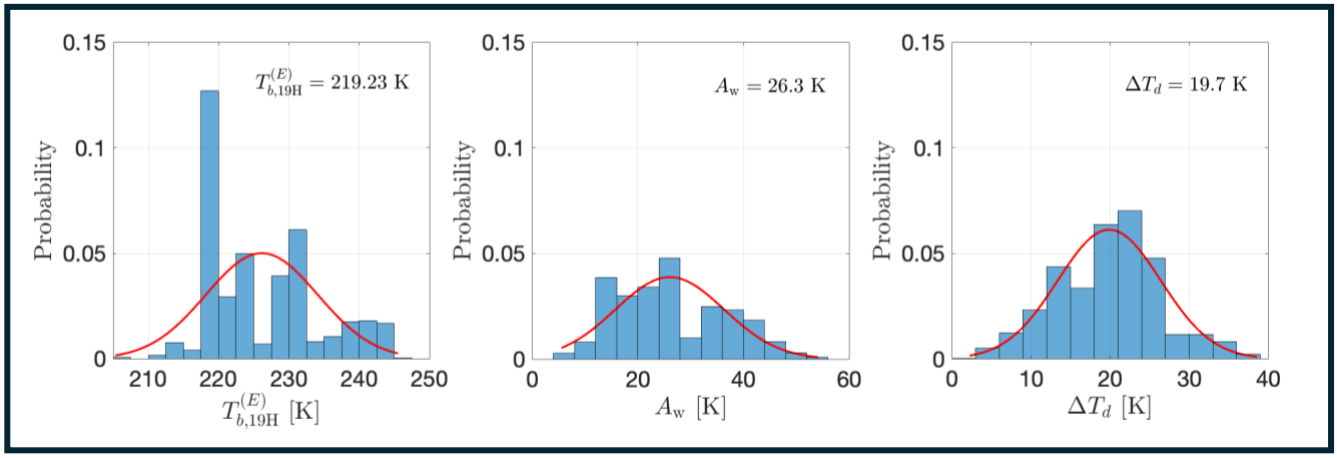

Figure S3: Distributions of threshold values for each indicator in the selected triplet, obtained from 1,000 Monte Carlo trials (random 30% melt days, 30% non-melt days per trial) under the majority decision rule. Histograms of the thresholds are shown for the three variables, with superimposed Gaussian fits illustrating their near-Gaussian shape.

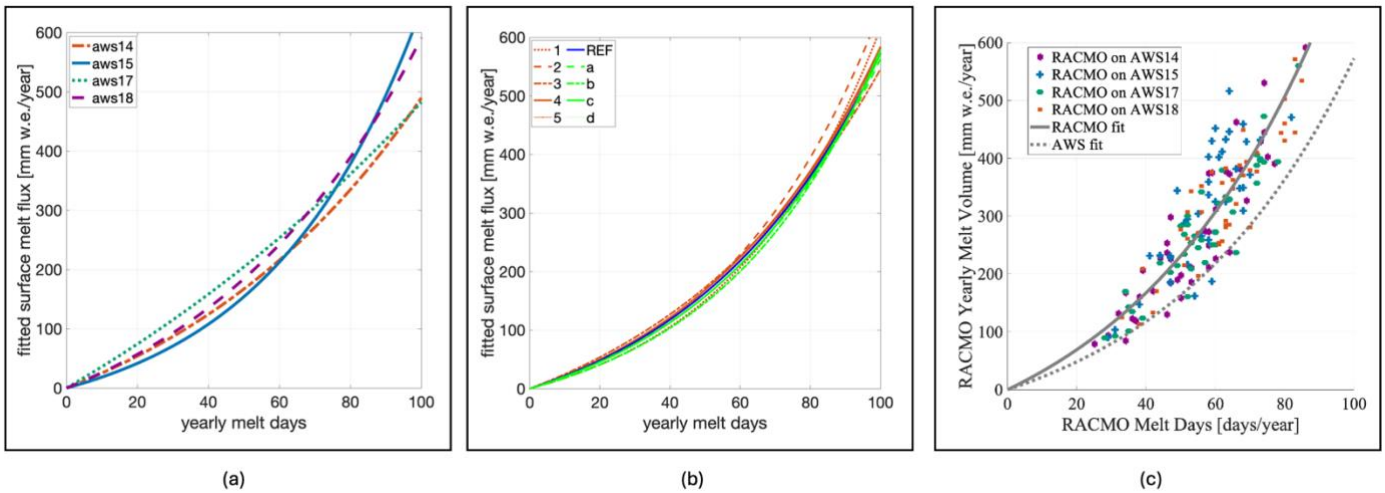

Figure S4: (a) Exponential melt-day to melt-volume relationship evaluated at each of the four AWS locations (AWS14, AWS15, AWS17, AWS18) where the sensitivity analysis was conducted.
(b) Exponential melt-day to melt-volume relationship computed for all AWS locations combined, using each of the 10 model-setup permutations from the sensitivity analysis. (c) Comparison of the AWS-derived melt-day to melt-volume relationship curve (dotted grey line) against RACMO2.4p1 outputs (solid grey line) at each AWS location involved in the sensitivity analysis.

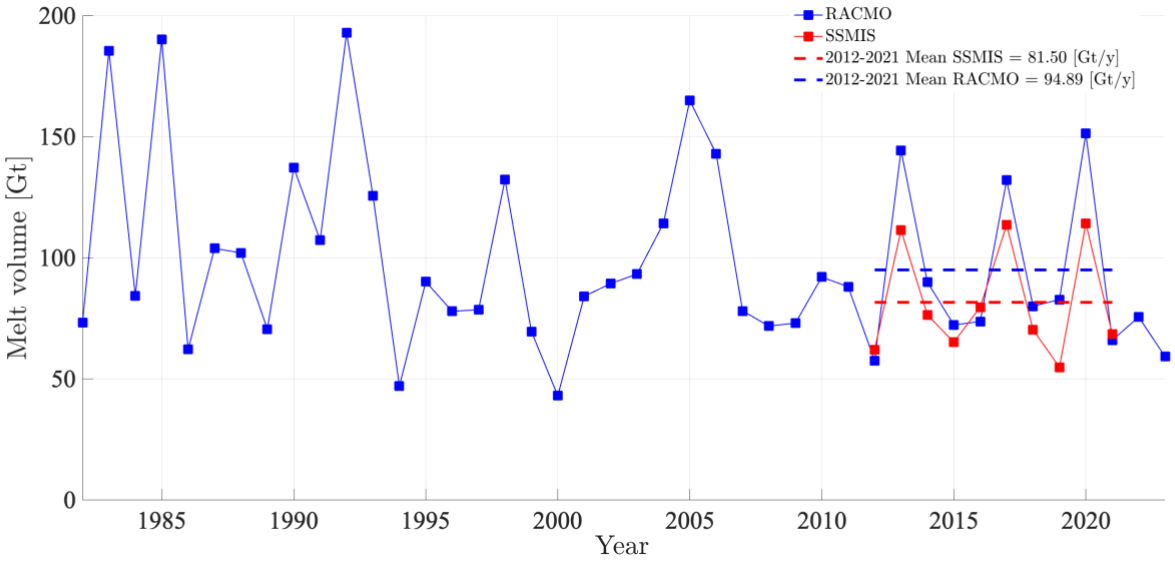

Figure S5: Total Antarctic-wide surface melt volume from SSMIS satellite retrievals and RACMO2.4p1 model output over the period 2012–2021 and 1980–2024, respectively. Dashed lines show melt means over 2012–2021 period.

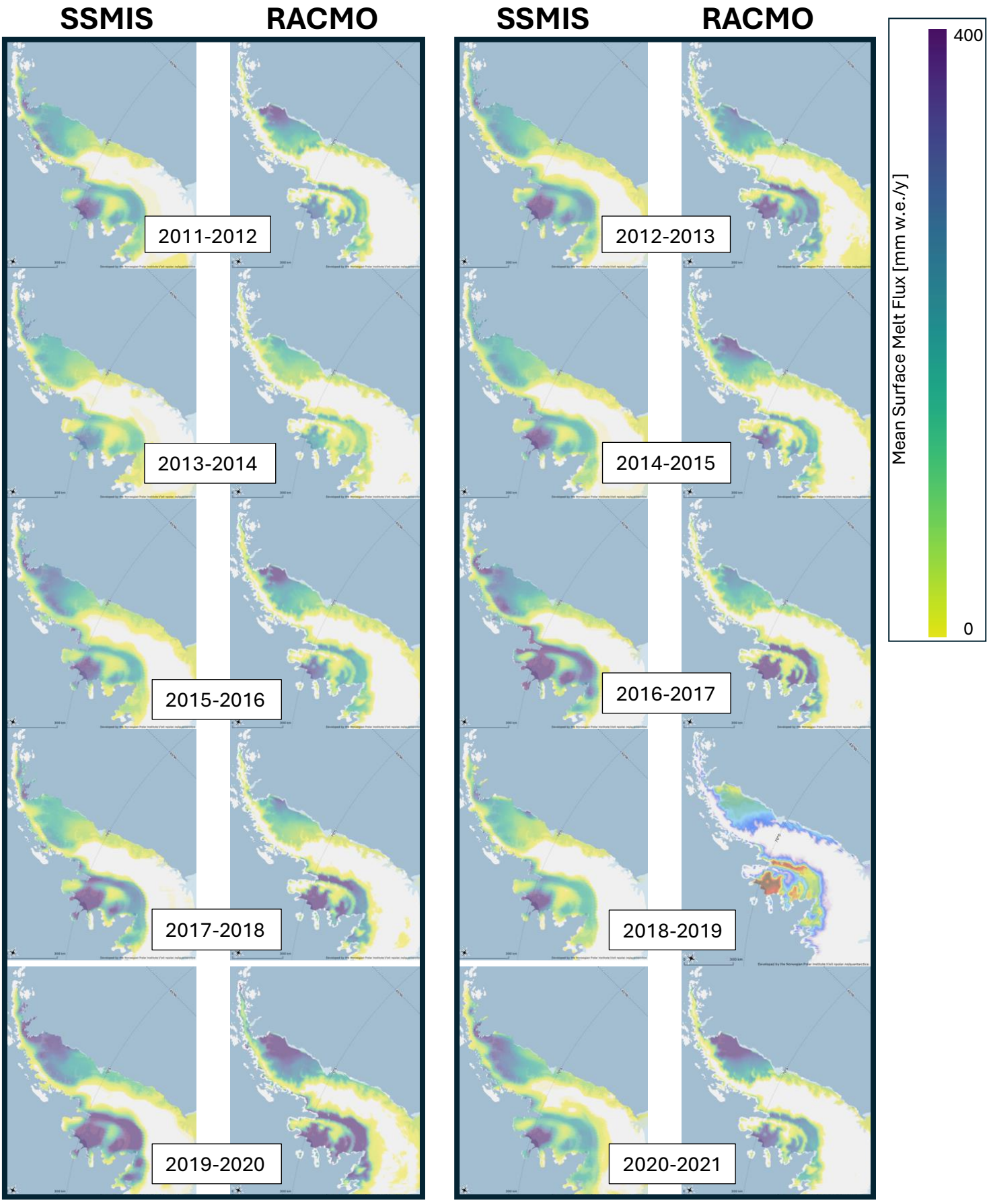

Figure S6: Comparison of regional (Antarctic Peninsula) annual mean surface melt flux maps derived from SSMIS and RACMO2.4 over the period from June 2011 to May 2021.

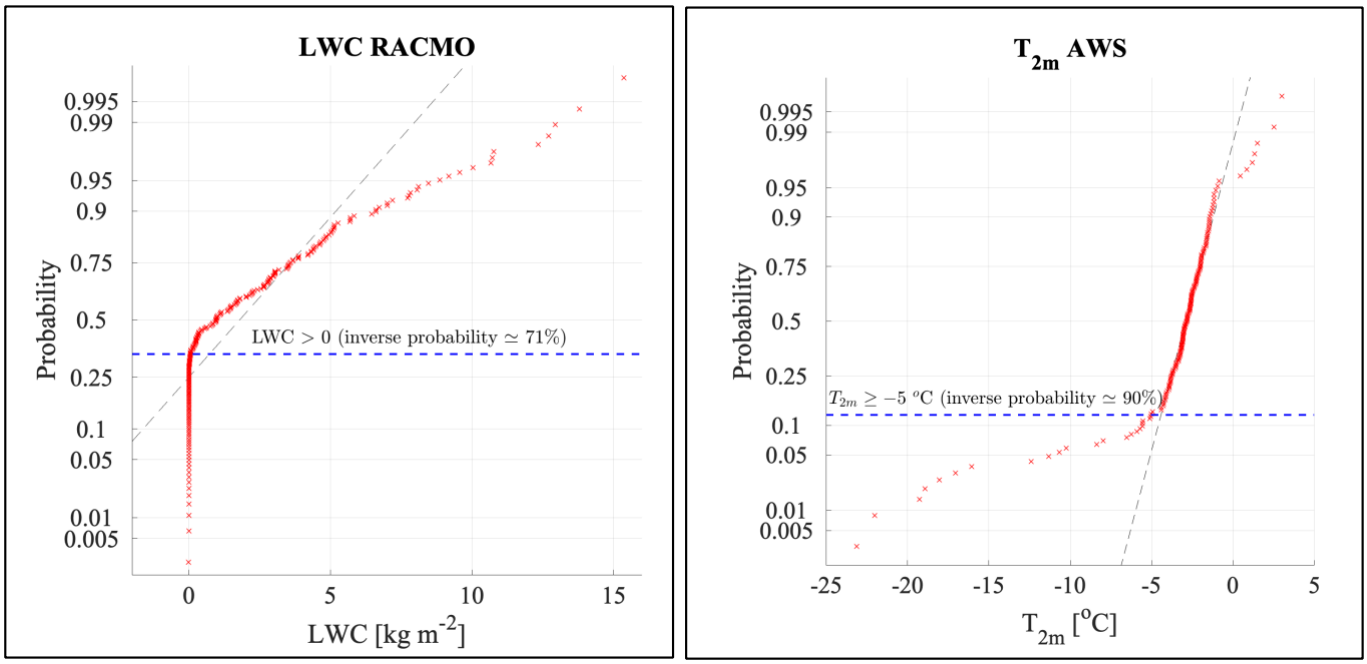

(a) (b)

Figure S7: (a) Probability distribution of LWC values from RACMO2.4p1 for false positive (melt-day misclassification) events, showing that approximately 71 % of the distribution lies at LWC > 0. (b) Probability distribution of AWS near-surface air temperature (T_{2m}) values for false positive events, indicating that roughly 90 % of the distribution lies at $T_{2m} \geq -5$ °C.